

Supporting information

Translocation of Enzymes in a Mesoporous MOF for Enhanced Catalytic Activity Under Extreme Conditions

José Navarro-Sánchez,^a Neyvis Almora-Barrios,^a Belén Lerma-Berlanga,^a J. Javier Ruiz-Pernía,^b Victor A. Lórenz-Fonfría,^a Iñaki Tuñón^b and Carlos Martí-Gastaldo^{*a}

^a Instituto de Ciencia Molecular (ICMol) Universidad de Valencia Catedrático José Beltrán-2, 46980, Paterna (Spain)

^b Departamento de Química Física Universidad de Valencia Doctor Moliner-50, 46100, Burjassot (Spain)

E-mail: carlos.marti@uv.es

Table of Contents

S1. Experimental section	3
Materials and reagents.	3
Experimental procedure.	3
Physical characterization.	3
S2. Enzyme size and MOF stability in different buffers	5
Figure S1. Dynamic light scattering (DLS) of protease in the medium used for infiltration.	5
Figure S2. Effect of the buffer over the structure of MIL-101(Al)-NH ₂ during enzyme infiltration.	5
S3. Computational information	6
Figure S3. Results of MD simulations of the Aspartic proteinase from <i>Aspergillus saitoi</i>	6
S4. Physicochemical characterization of the biocomposite	7
Figure S4. Fluorescent spectroscopy	7
Figure S5. Raman spectra of protease, MIL-101(Al)-NH ₂ and protease@MIL-101(Al)-NH ₂	8
Figure S6. PXRD of non-functionalized MIL-101(Cr).	9
Figure S7. UV-Vis of MIL-101(Cr) after incubation with protease in presence of Gly-Tyr.	9
Figure S8. Thermogravimetric analysis of the MIL-101(Al)-NH ₂ , protease@MIL-101(Al)-NH ₂ and free protease.	10
Figure S9. Evaluation of enzyme loading by UV-Vis spectroscopy of the supernatant after material washing.	10
Figure S10. Powder x-Ray diffraction and Le Bail refinements of MIL-101(Al)-NH ₂ and protease@MIL-101(Al)-NH ₂	11
Figure S11. Scanning Electron Microscopy (SEM).	12
S5. Proteolytic activity tests	13
Influence of the substrate concentration on the kinetics of peptide hydrolysis.	13
Figure S12. Hanes-Woolf curve of proteolytic activity	13
Figure S13. Effect of the pH over the proteolytic activity of protease (a) and protease@MIL-101(Al)-NH ₂ (b) at 25°C.	14
Figure S14. Effect of temperature over the proteolytic activity of protease (top) and protease@MIL-101-NH ₂ (bottom) at pH 7.4.	15
Figure S15. PXRD of protease@MIL-101(Al)-NH ₂ after the recyclability tests.	16
Figure S16. Activity of GOx alone (top), in presence of protease@MIL-101(Al)-NH ₂ (middle) and free protease (bottom) at room temperature in a buffered medium.	16
S6. References	18

S1. Experimental section

Materials and reagents.

All reagents and solvents used were of commercially available grade and used without any additional purification. Protease (from *Aspergillus saitoi* Type XIII, ≥ 0.6 unit/mg solid), Glucose Oxidase (from *Aspergillus niger* Type II, $\geq 15,000$ units/g solid), Azocasein (protease substrate), Glycyl-L-tyrosine (Gly-Tyr), 2-Aminoterephthalic acid (99%), Aluminium chloride hexahydrate ($\geq 98\%$), dimethyl formamide (DMF), buffers (TRIS base, HEPES, carbonate and PBS at 0.1 M) and other chemicals were used as acquired from commercial suppliers.

Experimental procedure.

Synthesis of MIL-101(Cr). The MOF was synthesized following a reported procedure¹. The solid was cleaned by centrifugation three times with fresh DMF and ethanol. The polycrystalline powder was then activated by Soxhlet extraction with ethanol overnight and dried under vacuum.

Synthesis of MIL-101(AI)-NH₂. The MOF was synthesized by following a reported procedure:² 2-aminoterephthalic acid (3.75 mmol) was dissolved in DMF (150mL) and heated up to 110°C. Then 7.5 mmol of aluminium chloride hexahydrate were added. The temperature was maintained constant four hours with magnetic agitation. The flask was tightly sealed and placed in an oven at 110°C for 16 hours. After cooling down to room temperature, the yellow precipitate was isolated by filtration and washed thoroughly with DMF, ethanol and acetone. The polycrystalline powder was then activated by Soxhlet extraction with ethanol overnight and dried under vacuum.

Synthesis of protease@MIL-101(AI)-NH₂. For the infiltration of the enzyme, 20 mg of protease were dissolved in 3 mL of TRIS buffer (0.1 mol L⁻¹, pH 7.4) followed by the addition of 60 mg of the activated MOF with continuous stirring. Then, 30 mL of anhydrous hexane were added to the incubation medium, that was maintained at 60 °C overnight. The mixture was next cooled down to 25 °C with continuous stirring for 1 hour. Protease@MIL-101(AI)-NH₂ was then isolated by centrifugation and washed abundantly with fresh aliquots of TRIS in order to remove the excess of non-infiltrated enzyme. The total uptake of protease by the MOF was evaluated by correlating the disappearance of the UV-Vis band of the enzyme at 260 nm in the supernatant with its decreasing concentration in solution upon washing. The solid was dried at 50 °C under dynamic vacuum to obtain a yellowish powder that was stored at 4 °C for activity tests.

Proteolytic activity tests. The catalytic activity of protease@MIL-101(AI)-NH₂ was typically tested for 20 mg of the solid incubated at room temperature with 20 μ mol of Glycyl-L-tyrosine (GlyTyr) in 3 ml of TRIS buffer (0.1M, pH 7.4) and compared to 1 mg of the free enzyme in the same medium, that was used as a reference. The evolution of the intensity of the UV-Vis band representative of the peptide with time at 5, 10, 15, 30, 60, 120, 180 and 300 minutes was measured at 285 nm and plotted for the calculation of the catalytic activity and analysis of the enzyme kinetics. Aliquots of 100 μ L were taken for the UV-Vis experiments. Variations in the catalytic activity with temperature and pH were analyzed by carrying out the same experiment. Temperature was controlled in a heating bath between 25 and 125 °C. pH was buffered between 1 and 12 by using a concentrated solution of HCl and NaOH. Reusability tests were performed by using 40 mg of protease@MIL-101(AI)-NH₂ in a normal proteolytic procedure, followed by cleaning with aliquots of TRIS in each cycle.

GOx (Glucose oxidase) interference tests. The compatibility of protease with competing enzymes like GOx before and after encapsulation was studied by using either 20 mg of the biocomposite or 1 mg of the free enzyme incubated at room temperature with 20 μ mol of Glucose in 3 ml of TRIS buffer. The reduction of the intensity of the UV-Vis band representative of the glucose was measured and plotted for the calculation of the catalytic activity from aliquots extracted from the reaction medium between 0 and 180 minutes. The reactions were performed at pH 7.4.

Fluorescence spectroscopy. Solution emission studies of free protease and protease@MIL-101(AI)-NH₂ were performed using 5 mg of fresh material suspended in 3 mL of TRIS buffer in a 1 cm quartz optical cuvette using a TI-Fluorimeter equipped with a GL-3300 nitrogen laser, a GL-302 dye laser and a photomultiplier detection system. The sample was continuously stirred during the measurements. For the temperature with hexane-water experiments were used 2.85 mL of hexane and 0.15 mL of TRIS buffer, and all the samples were heated inside the tray and immediately measured. The excitation wavelength for all studies was 276 nm.

Raman spectroscopy. Solution emission studies of free protease and protease@MIL-101(AI)-NH₂ were performed using 5 mg of fresh material over a glass slide. All experiments have been repeated at least five times to confirm reproducibility.

Physical characterization.

Dynamic light scattering (DLS) measurements were carried out with a Zetasizer Nano ZS instrument (Malvern Instruments Ltd.) on a fresh solution of the enzyme in TRIS buffer (1 g.L⁻¹). The temperature was set at 25 \pm 0.1 °C using a thermostat bath. The mean hydrodynamic diameter was determined by accumulative analysis. UV-Vis spectra were measured with a spectropolarimeter Jasco J-810 and recorded from a temperature of 25°C. Ellipticity values were recorded every 0.5 nm at a wavelength scanning speed of 20 nm/min. The response time was set to 1s and the bandwidth was set to 1 nm. The final spectrum represented the accumulate average of three consecutive scans. Powder X-ray diffraction (PXRD) was collected in a PANalytical X'Pert PRO diffractometer using copper radiation (Cu K α = 1.5418 Å) with an X'Celerator detector, operating at 40 mA and 45 kV. Profiles were collected in the 2° < 2 θ < 40° range with a step size of 0.017°. Phase purity of the solid before/after enzyme infiltration was confirmed by Le Bail refinement with the

FULLPROF software package.³ Particle morphologies and dimensions were studied in a Hitachi S-4800 scanning electron microscope (SEM) at an accelerating voltage of 15 keV, over metalized samples with a mixture of gold and palladium during 30 s. Gas adsorption measurements were recorded in a Micromeritics 3Flex at relative pressures up to 1 bar and performed ex-situ on activated solids. Samples were degassed overnight at 100 °C and 10⁻⁶ Torr prior to analysis. Nitrogen adsorption-desorption isotherms were recorded at 77 K. Specific surface areas were calculated using the Brunauer–Emmett–Teller (BET) method in the relative pressure range $P/P_0 = 0.05–0.30$. The pore size distribution was analyzed by using a non-linear density functional theory (NLDFT) methods for the adsorption branch by assuming a cylindrical pore model. FT-IR was collected in the 4000–400 cm⁻¹ range from ground microcrystalline powder using an ATR Agilent Cary 630. Thermogravimetric analysis (TGA) was carried out with a Mettler Toledo TGA/SDTA 851e apparatus between 25 and 600 °C under ambient conditions (10 °C·min⁻¹ scan rate and an air flow of 30 mL·min⁻¹). All the Raman experiments were carried out using Confocal Raman Microscope purchased from Horiba-MTB Xplora in the range from 200 to 3600 cm⁻¹. A laser at 532 nm was used with a power of 0.0074mW at room temperature. The Raman shift was calibrated using silicon. All samples were placed on a glass slide, with 40 accumulations of 2 seconds each. The spectrograph grating was 600 grooves/mm and a 10X objective was used.

S2. Enzyme size and MOF stability in different buffers.

Figure S1. Dynamic light scattering (DLS) of protease in the medium used for infiltration.

DLS measurements were carried out with a Zetasizer Nano ZS instrument (Malvern Instruments Ltd.) on a fresh solution of the enzyme in TRIS buffer (1 g.L⁻¹; pH 7.4) at 25 °C. The mean hydrodynamic diameter of 2.85 nm was determined by statistic analysis of five different samples.

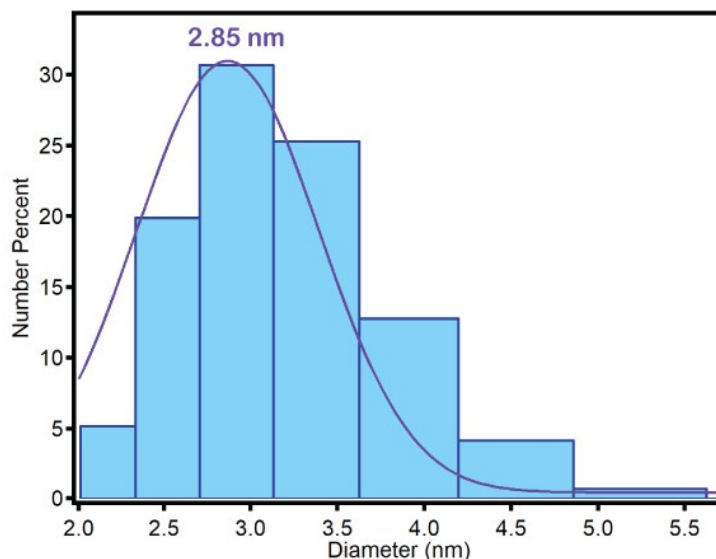
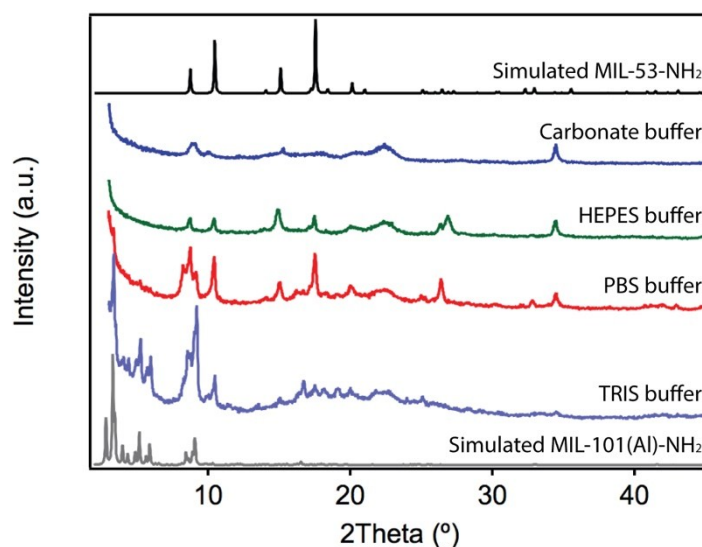


Figure S2. Effect of the buffer over the structure of MIL-101(Al)-NH₂ during enzyme infiltration.

Powder x-Ray diffraction (PXRD) of MIL-101(Al)-NH₂ displays important changes in presence of saline phosphate (PBS), sulphonate (HEPES) and carbonate buffers. Previous reports also confirm the negative influence of PBS over the structure of MIL-100(Fe) and the good of TRIS buffer.^{4,5} In turn, the structure of the MOF is retained for an amine buffer (PBS), highlighting the importance of an adequate buffer to preserve the structural integrity of the MOF during enzyme infiltration. For comparison, the same experimental conditions described in the experimental section of the manuscript were used for the four different buffers. After thorough washing with fresh aliquots of the corresponding buffer, PXRDs of the solids isolated were collected in a PANalytical X'Pert PRO diffractometer using copper radiation (Cu K_α = 1.5418 Å) with an X'Celerator detector, operating at 40 mA and 45 kV. Profiles were collected in the 2° < 2θ < 45° range with a step size of 0.02°.

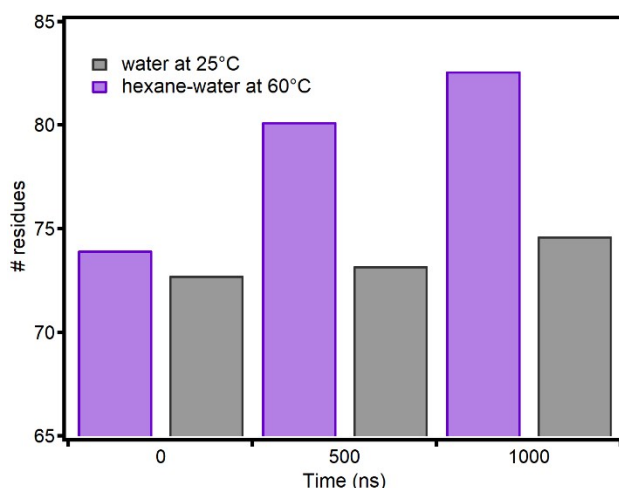


S3. Computational information.

The initial coordinates were taken from the X-ray crystal structure of Aspergillopepsin I (AP) from *Aspergillus saitoi* (also known as *Aspergillus Phoenicis*). The structure employed can be found in *Protein Data Bank* under the filename 1IBQ.⁶ AP from *Aspergillus saitoi* is a monomer with one active site and a total of 325 residues. The protonation state of each residue was determined at pH=7 employing PROPKA 3.1 program.⁷ Classically, all atom solvation was added explicitly with molecular dynamics simulation for the three systems: *i*) protein in water at 25°C, *ii*) protein in water at 60°C and *iii*) protein in a 3:1 mixture of hexane:water at 60°C were performed using GPU version of PMEMD engine integrated with Amber16 package.⁸ The LEAP program of AMBER16 was used to generate topologies for the systems and add missed hydrogen atoms. The protein was then solvated in a cubic box of water molecules (aqueous systems) and hexane:water box (mixed system) with a 10 Å buffer region in all directions from the protein. 23 sodium ions were added to neutralize the systems. The hexane:water mixture box was generated using PACKMOL program.⁹ The protein, sodium ions and hexane were described using AMBER force field¹⁰ while explicit water molecules were described by means of the TIP3P classical potential.^{11,12} Energy was minimized by the steepest descent method with weak constraints for 10000 steps. Systems were subsequently heated up to 25°C and 60°C for the aqueous systems and 60°C in the case of the hexane:water mixture. Afterwards, the three systems were equilibrated under 1 bar pressure over 100 ns in the isothermal-isobaric ensemble (NPT: a constant number of particles, constant pressure and constant temperature). Finally, 1 μ s of production were performed on the three systems by using periodic boundary conditions. The Particle Mesh Ewald (PME) method implemented in AMBER16, with direct space and a Van der Waals cut-off of 10 Å, was used to treat long-range electrostatic interactions. The SHAKE algorithm¹³ was employed to constraint bonds involving hydrogen atoms, which allowed the use of a 2 fs timestep. The Langevin algorithm¹⁴ was applied to couple systems to a 25 and 60°C external temperature bath. Finally, trajectories analysis including the Root Mean Square Deviation (RMSD), radius of gyration and secondary structure analysis were carried out using CPPTRAJ¹⁵ modules as implemented in AMBER16. Analysis of the secondary structure was carried out using the DSSP method.¹⁶ The average number of residues belonging to unstructured regions (see Figure S3 below) was obtained as the difference between the total number of residues of the protein (325) and the average number of residues assigned to different secondary motifs by DSSP. Averages were taken in blocks of 100 ns.

Figure S3. Results of MD simulations of the Aspartic proteinase from *Aspergillus saitoi*.

Average number of residues belonging to regions without secondary structure for the protein in hexane:water at 60°C (purple) and in water at 25°C (black). As time passes, the number of residues that do not have a defined structure increases for hexane-water, whereas on only water remains unchanged. Only when hexane is added into the calculations there is a boost on randomly structured regions.



S4. Physicochemical characterization of the biocomposite.

Figure S4. Fluorescent spectroscopy

Fluorescent spectra of the fully re-assembled protein (maintained overnight at 80°C, in purple) compared with the original free enzyme (black). Also included the spectra of the MIL-101(Al)-NH₂ to confirm that it does not interfere with the emission of the enzyme.

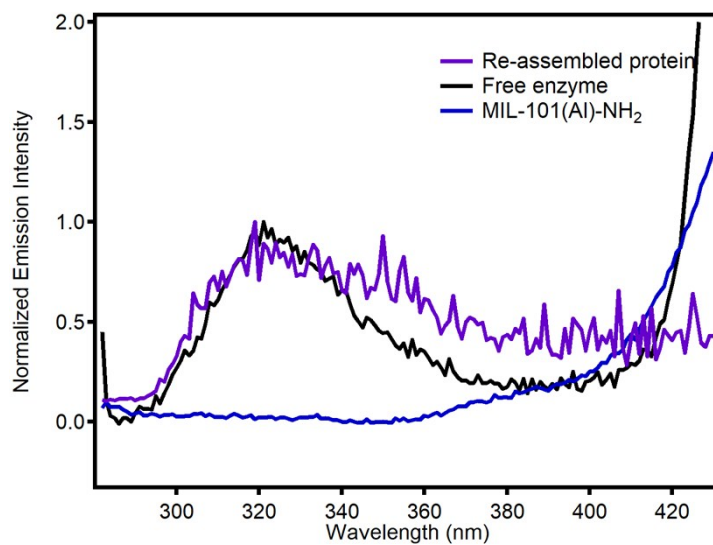


Figure S5. Raman spectra of protease, MIL-101(Al)-NH₂ and protease@MIL-101(Al)-NH₂.

Raman spectra of the free enzyme (purple), MIL-101(Al)-NH₂ (black) and protease@MIL-101(Al)-NH₂ (blue) in solid. The bands at 490 and 2430 cm⁻¹ correspond to the vibration of disulfide bonds intrinsic to the cysteines in the polypeptide sequence of protease (UniProt code Q12567). a. Full spectra from 230 to 3600 cm⁻¹ with the Raman peaks associated to the protein marked with grey bars. b. Zoom-in of the bands between 430-520 and c. 2350-2500 cm⁻¹. The signals at 470 and 2436 cm⁻¹ in the enzyme are blue shifted close to 6 and 9 cm⁻¹ after encapsulation as result of the interaction with the framework.

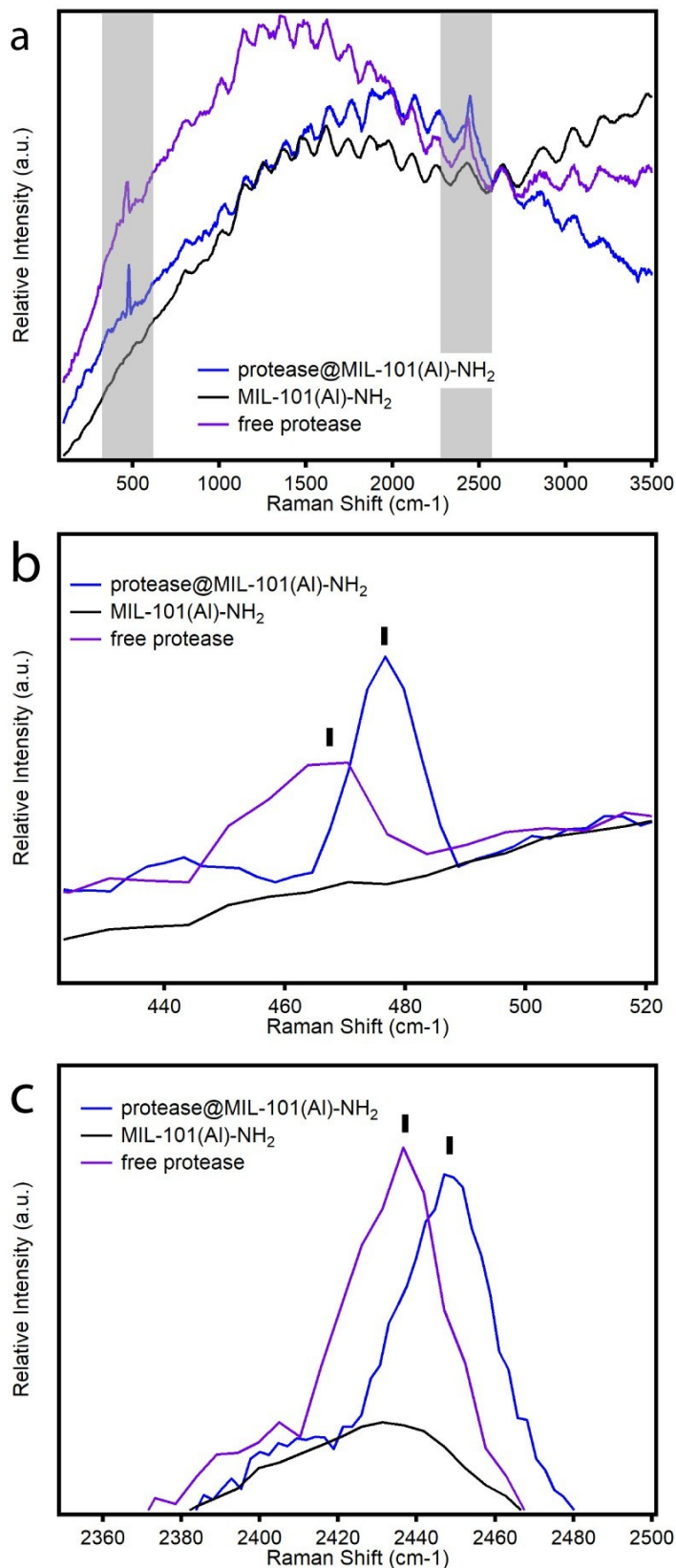


Figure S6. PXRD of non-functionalized MIL-101(Cr).

PXRDs of MIL-101(Cr) simulated (black) and as-synthesized material (green).

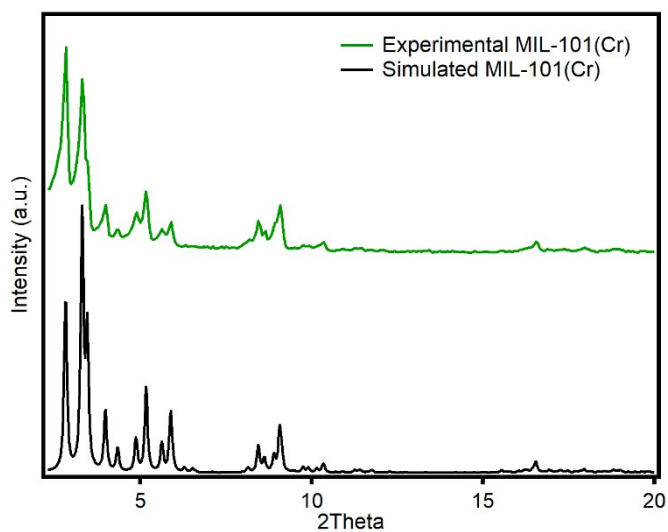


Figure S7. UV-Vis of MIL-101(Cr) after incubation with protease in presence of Gly-Tyr.

Evolution of the proteolytic activity of MIL-101(Cr) after incubation with protease with time. Activity was followed with UV-Vis by monitoring the increase in absorption of the band intrinsic to the peptide (285 nm). For this essay we used 20 mg of the incubated solid (following the same procedure as for the MIL-101(Al)-NH₂) and 10 mg of GlyTyr dipeptide as substrate on 3 mL of TRIS buffer. As confirmed by the constant absorption value collected between 0 and 180 min, there was no measurable activity after the cleanings that could be linked to the presence of encapsulated enzyme. This confirms the importance of -NH₂ groups in MIL-101(al)-NH₂ to favour the translocation and subsequent regeneration of an active conformation of the enzyme into the MOF.

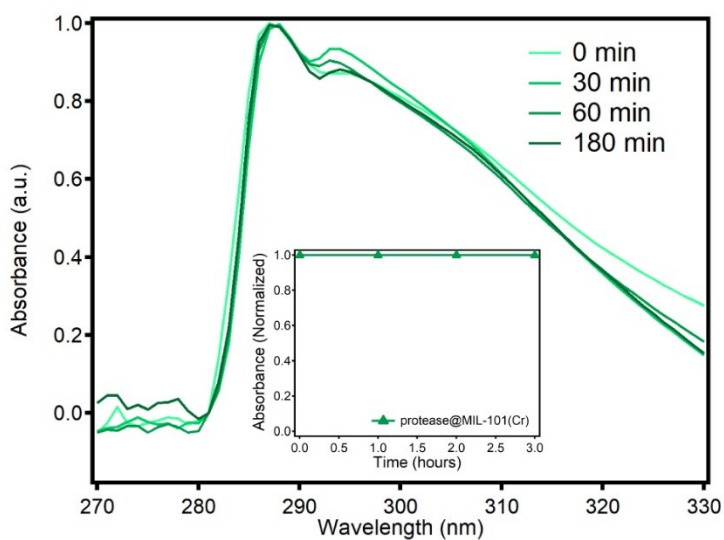


Figure S8. Thermogravimetric analysis of the MIL-101(Al)-NH₂, protease@MIL-101(Al)-NH₂ and free protease.

Thermogravimetric analysis (TGA) was carried out with a Mettler Toledo TGA/SDTA 851e apparatus between 25 and 600°C under ambient conditions (10°C·min⁻¹ scan rate and an air flow of 30 mL·min⁻¹). The solids were measured after activation to minimize the effect of solvent loss over the TGA. Grey area stands for the decomposition of the protease inside the MOF. The decomposition of the free protease starts at 250°C, where protease@MIL-101(Al)-NH₂ also displays a slight weight loss, not present in the MOF before encapsulation, that corresponds approximately to 5% of mass loss.

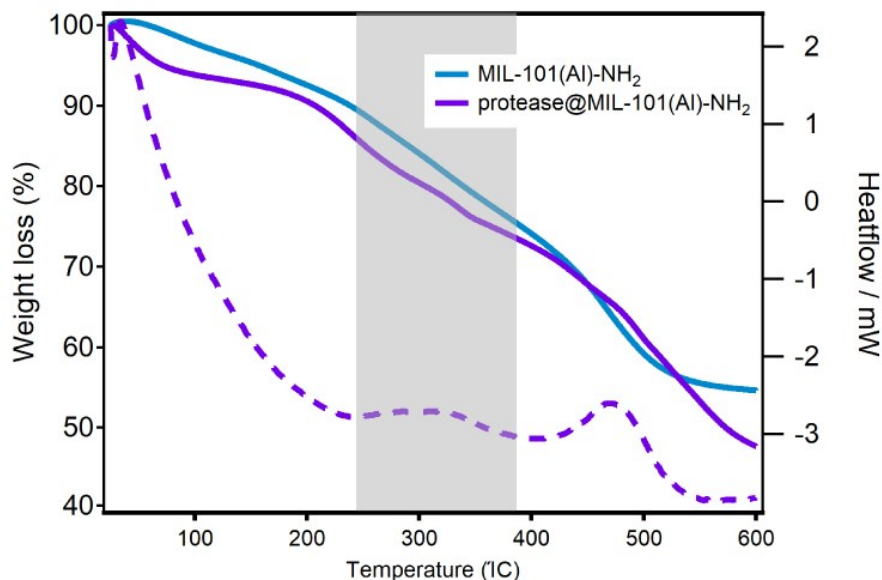


Figure S9. Evaluation of enzyme loading by UV-Vis spectroscopy of the supernatant after material washing.

UV-Vis spectra were measured with a spectropolarimeter Jasco J-810 and recorded at 25°C. Ellipticity values were recorded every 0.5 nm at a wavelength scanning speed of 20 nm/min. The response time was set to 1s and the bandwidth was set to 1 nm. The final spectrum represented the accumulate average of three consecutive scans. The uptake was calculated by correlating the drop in the absorption of the band intrinsic to protease, at 260 nm, with the concentrations of non-encapsulated enzyme in the supernatants after washing the material. The difference between the amount of enzyme detected in solution and the starting concentration accounts for close to 5% of uptake.

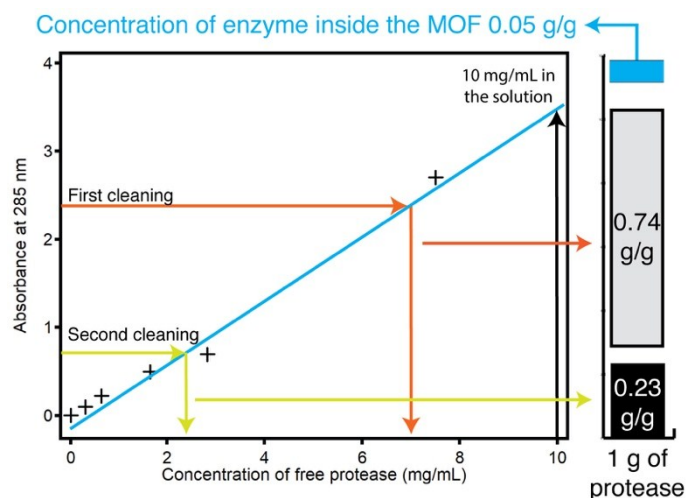


Figure S10. Powder x-Ray diffraction and Le Bail refinements of MIL-101(Al)-NH₂ and protease@MIL-101(Al)-NH₂.

Experimental (black line), calculated (red line), difference plot $[(\text{obs}-\text{calcd})]$ (blue line, bottom panel) and Bragg positions (green ticks, bottom panel) for the refinement of experimental diffraction data collected at room temperature of MIL-101(Al)-NH₂ before and after enzyme infiltration. PXRDs were collected in a PANalytical X'Pert PRO diffractometer using copper radiation (Cu K α = 1.5418 Å) with an X'Celerator detector, operating at 40 mA and 45 kV. Profiles were collected in the 2° < 2 θ < 40° range with a step size of 0.017° and refined with the FULLPROF software package¹⁷ by using CCDC605510 as a starting model.

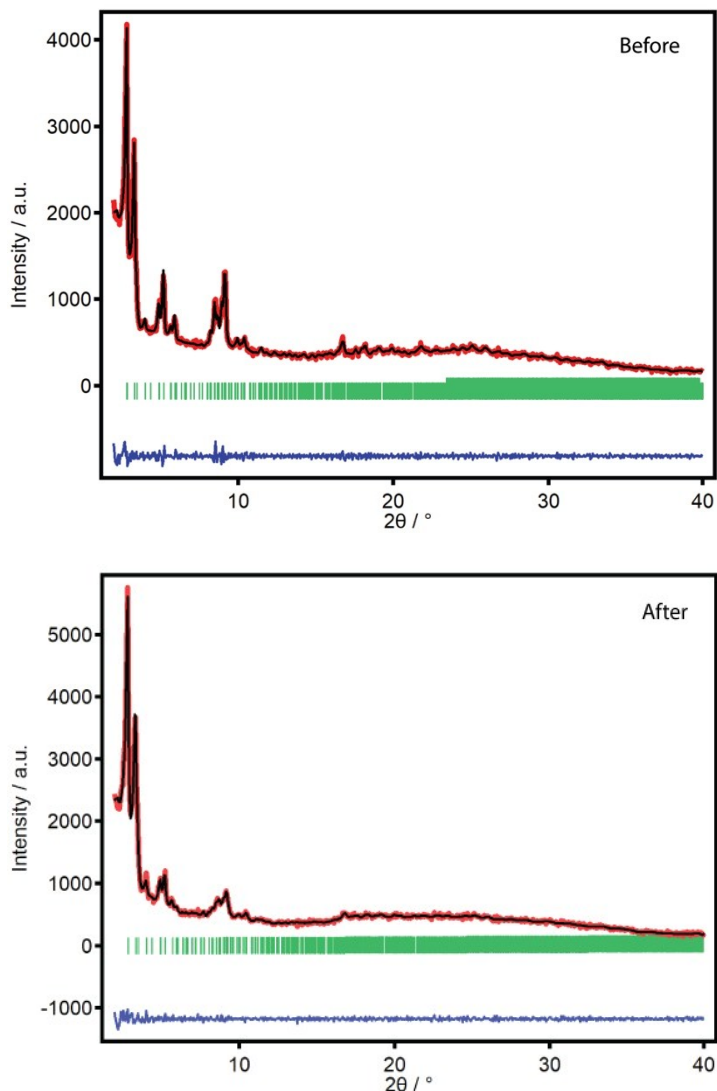
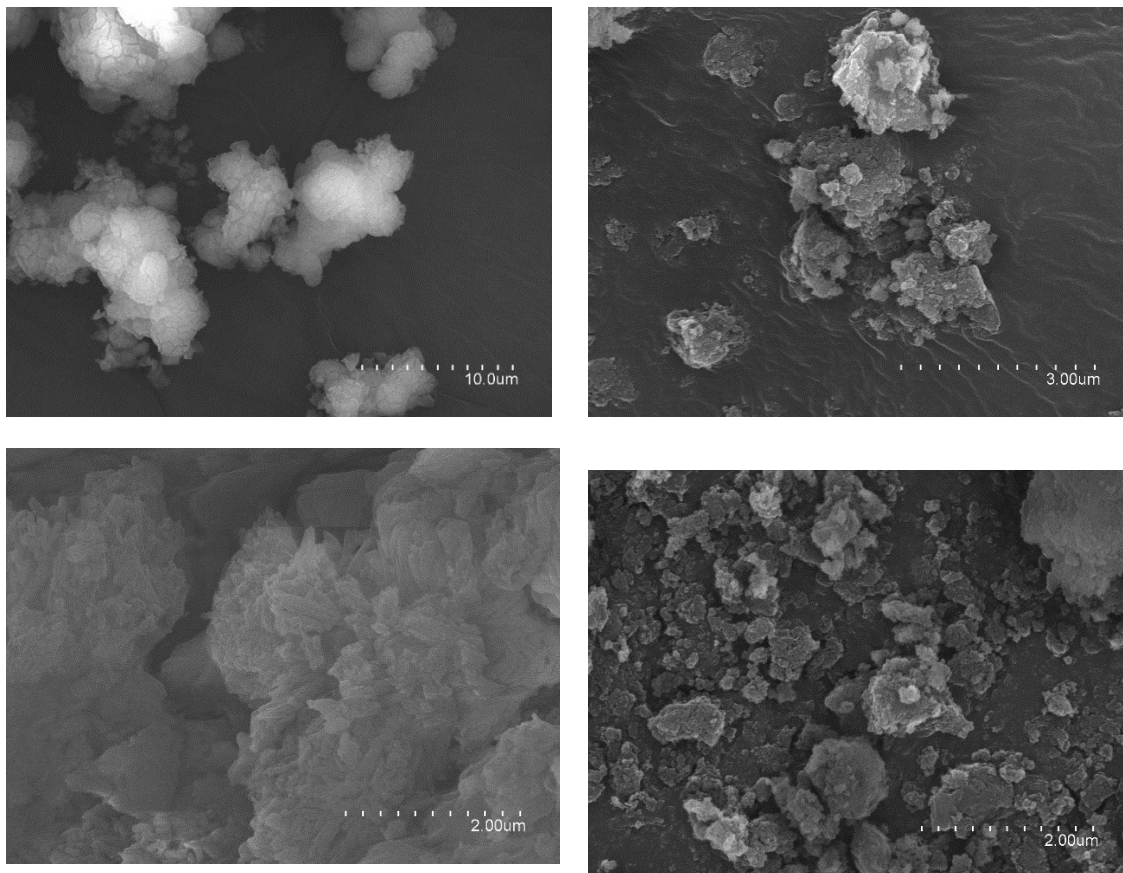


Table S1. Summary of the parameters obtained from the LeBail refinements.

	V [Å ³]	a [Å]	R _e [%]	R _p [%]	R _{wp} [%]	gof
MIL-101(Al)-NH ₂	680615.94	88.4	3.36	4.37	4.53	1.0
protease@MIL-101(Al)-NH ₂	680039.75	87.9	3.48	4.52	4.22	1.0

Figure S11. Scanning Electron Microscopy (SEM).

SEM images of as-made MIL-101(AI)-NH₂ (*top row*) and protease@MIL-101(AI)-NH₂ (*bottom row*). Particle morphologies and dimensions were studied with a Hitachi S-4800 scanning electron microscope at an accelerating voltage of 20 keV, over metalized samples with a mixture of gold and palladium during 30 s.



S5. Proteolytic activity tests.

Influence of the substrate concentration on the kinetics of peptide hydrolysis.

Kinetics of the proteolytic activity was studied by using 20 mg of protease@MIL-101(Al)-NH₂ and 1 mg of free protease separately with 1, 2, 3, 4, 6 and 8 mM of GlyTyr. Kinetic parameters of the enzyme before and after encapsulation were determined by fitting the experimental data to the Hanes-Woolf equation:¹⁸

$$\frac{[S]}{v} = \frac{[S]}{V_{MAX}} + \frac{K_M}{V_{MAX}}$$

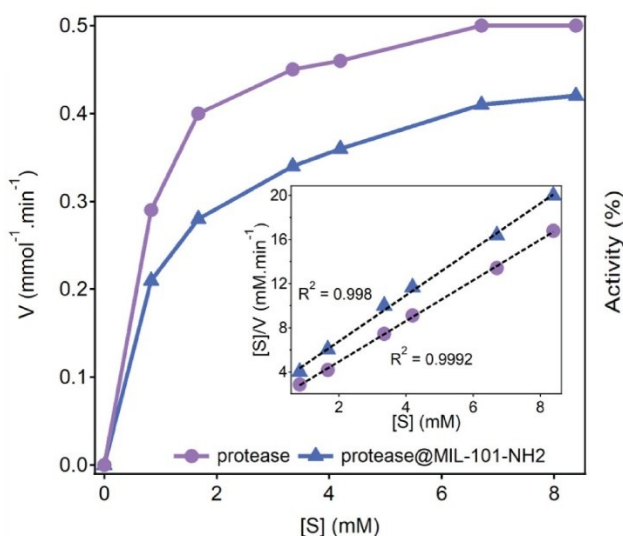
in which [S] represents the initial substrate concentration, v stands for the velocity of the reaction, V_{max} represents the maximum rate achieved by the system, at saturating substrate concentration, and K_M is the substrate concentration at which the reaction rate is half of the $V_{max} \cdot k_{cat}$, according to the equation:

$$k_{cat} = \frac{V_{max}}{[E_T]}$$

in which [E_T] represents the catalyst site concentration. It corresponds to the number of substrate molecules that each enzyme site converts to product per unit time (maximum efficiency). Finally, the ratio k_{cat}/K_M stands for the catalytic efficiency.¹⁹

Figure S12. Hanes-Woolf curve of proteolytic activity

The evolution of the proteolytic activity with time was followed with UV-Vis by monitoring the increase in absorption of the band intrinsic to the peptide (285 nm). First, we analyzed the kinetics of enzyme reactivity for the hydrolysis at pH 3 and 25 °C of different quantities of Gly-Tyr, ranging from 0.8 to 8.4 μmol, in the presence of 1 mg of free protease (blue) and 20 mg of protease@MIL-101(Al)-NH₂ (purple). These are the optimal working conditions for the alkaline protease used in this work.²⁰



The comparison of the calculated kinetics parameters is summarized in **Table S2**. Compared to the free enzyme under the same conditions, the initial hydrolysis rate of the peptide is slower for protease@MIL-101(Al)-NH₂ with a smaller k_M value. This is likely due to the slower diffusion of reactants and products in the MOF after loading. In turn, the biocomposite displays a higher K_{cat} value and k_{cat}/K_M ratios compared to the free enzyme, possibly due to the stability offered by the MOF. This suggests a change on the structure of the active site of the encapsulated enzyme, thus requiring a smaller Gly-Tyr concentration to achieve the maximum conversion rate. This behavior is consistent with previous works that report a similar effect on enzymatic reactivity after encapsulation in mesoporous MOFs.²¹ This can be correlated with the subtle change observed in the fluorescent measurements, as the structure of the protease inside the MOF is different from the native. A different arrangement of the tryptophan and tyrosine residues might imply a different structure of the active site and thus a different specificity and velocity of the enzymatic reaction performed.

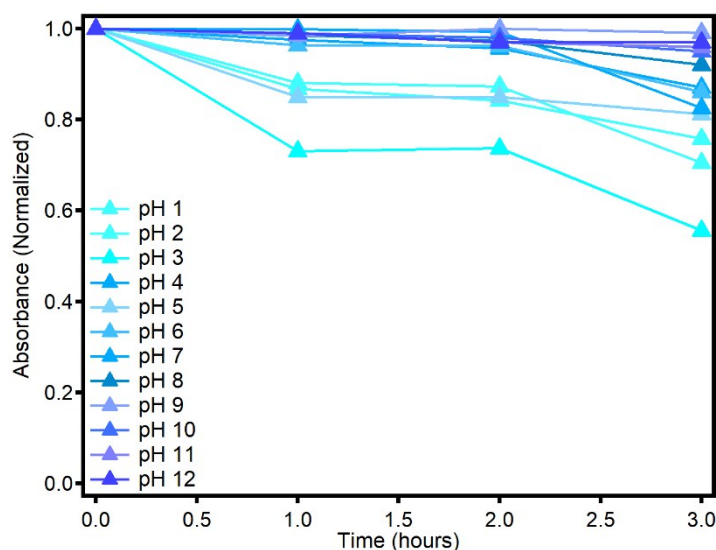
Table S2. Comparison of kinetic parameters for peptide hydrolysis of free and encapsulated protease in buffered conditions.

Protease	K_M (mM)	k_{cat} (min^{-1})	k_{cat}/K_M ($\text{min}^{-1}\text{mM}^{-1}$)
Free	1.01	45	45
Encapsulated	0.66	55	83

Figure S13. Effect of the pH over the proteolytic activity of protease (a) and protease@MIL-101(Al)-NH₂ (b) at 25°C.

For these essays we used 20 mg of the solid incubated at room temperature with 20 μmol of GlyTyr in 3ml of TRIS buffer and compared to 1 mg of the free enzyme in the same medium, that was used as a reference. The evolution of the intensity of the band representative of the peptide (285 nm) with pH was measured and plotted for the calculation of the catalytic activity from aliquots of 100 μL , extracted from the reaction medium at 0, 60, 120 and 180 minutes, after dilution in 2.9 mL of TRIS buffer. The reactions were performed at pH 1-12 and 25°C. pH was monitored in a pH-meter GLP-20 from CRISON and controlled by addition of concentrated solution of HCl and NaOH.

a) Protease



b) Protease@MIL-101(Al)-NH₂

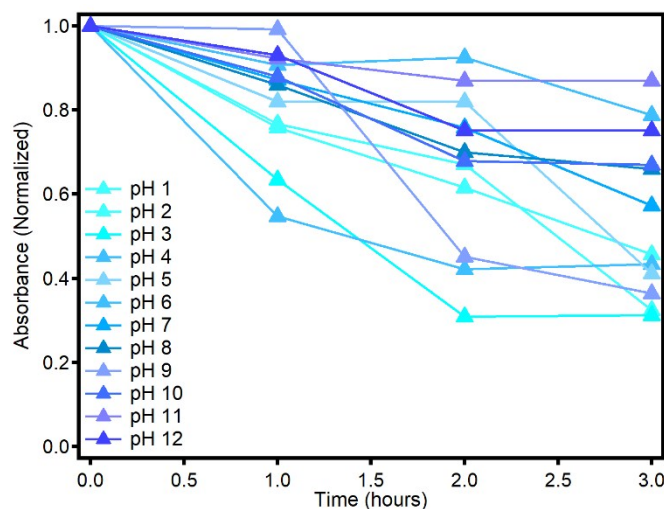
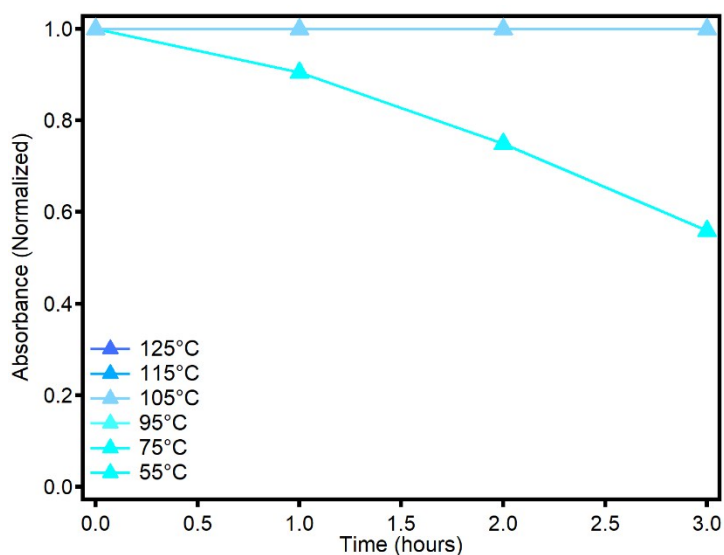


Figure S14. Effect of temperature over the proteolytic activity of protease (top) and protease@MIL-101-NH₂ (bottom) at pH 7.4.

For these essays we used 20 mg of the solid incubated at room temperature with 20 μ mol of GlyTyr in 3 ml of TRIS buffer and compared to 1 mg of the free enzyme in the same medium, that was used as a reference. The evolution of the intensity of the band representative of the peptide with temperature between 25 and 125°C was measured and plotted for the calculation of the catalytic activity from aliquots of 100 μ L, extracted from the reaction medium at 0, 60, 120 and 180 minutes, after dilution in 2.9 mL of TRIS buffer. The reactions were performed at pH 7.4. Temperature was controlled with a thermostat in a heating bath.

a) Protease



b) Protease@MIL-101(AI)-NH₂

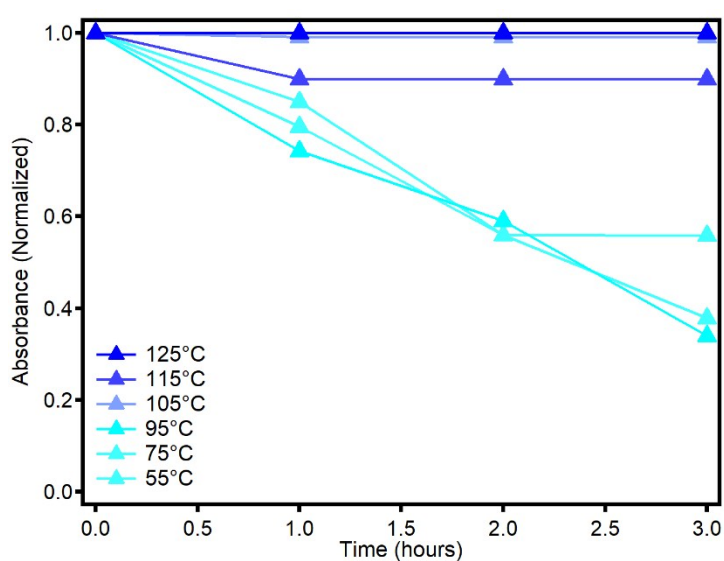


Figure S15. PXRD of protease@MIL-101(Al)-NH₂ after the recyclability tests.

Comparison of the PXRD of protease@MIL-101(Al)-NH₂ after the recyclability tests run at 25°C, pH 7.4 (light blue) and 95°C, pH 2.0 (purple) with the simulated pattern of MIL-53-NH₂ (black; CCDC647506) and MIL-101-NH₂ (grey, CCDC605510). The biocomposite retains its structural integrity at room temperature. However, heating at 95°C in an acid medium causes a structural transformation into the MIL-53 phase consistent with the appearance of characteristic Bragg peaks: [011], [020], [101] and [022]. This is possibly the reason for the gradual decrease in activity upon cycling as result of the leaching of the enzyme.

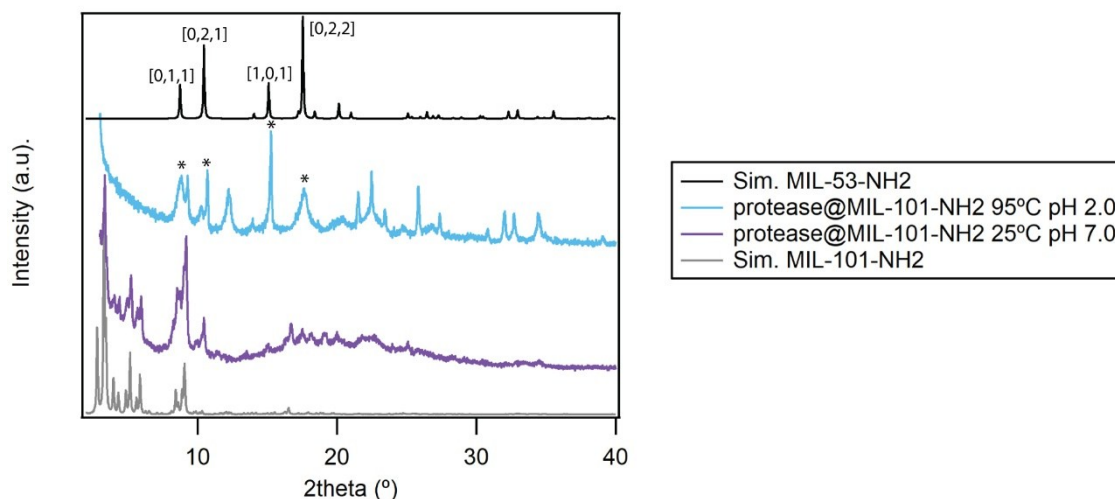
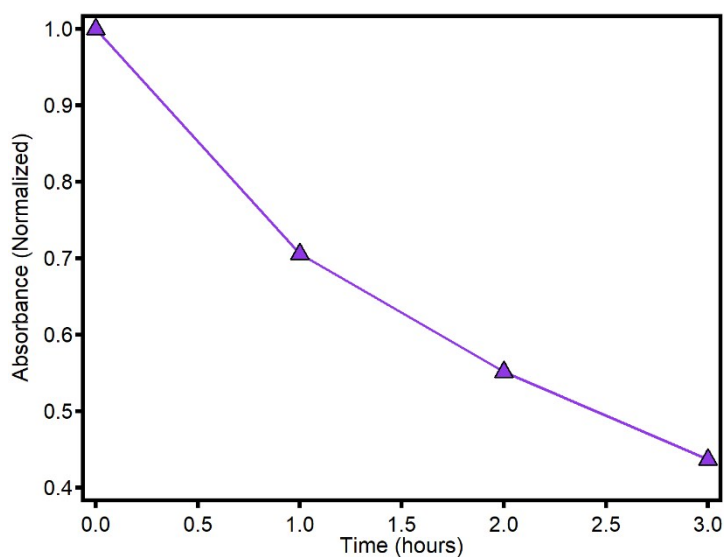


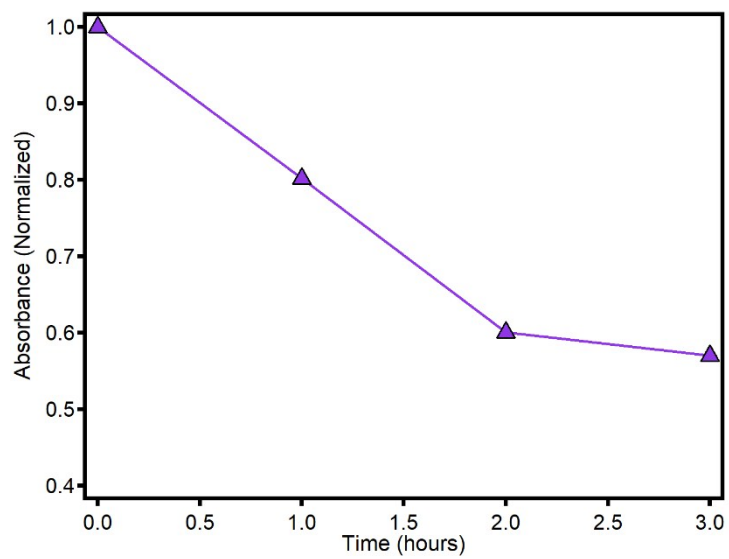
Figure S16. Activity of GOx alone (top), in presence of protease@MIL-101(Al)-NH₂ (middle) and free protease (bottom) at room temperature in a buffered medium.

For these essays we used 20 mg of the solid incubated at room temperature with 20 μmol of Glucose in 3 ml of TRIS buffer and compared to 1 mg of the free protease in the same medium, that was used as a reference. The reduction of the intensity of the UV-Vis band representative of the glucose was measured and plotted for the calculation of the catalytic activity from aliquots of 100 μL, extracted from the reaction medium at 0, 60, 120 and 180 minutes, after dilution in 2.9 mL of TRIS buffer. The reactions were performed at pH 7.4.

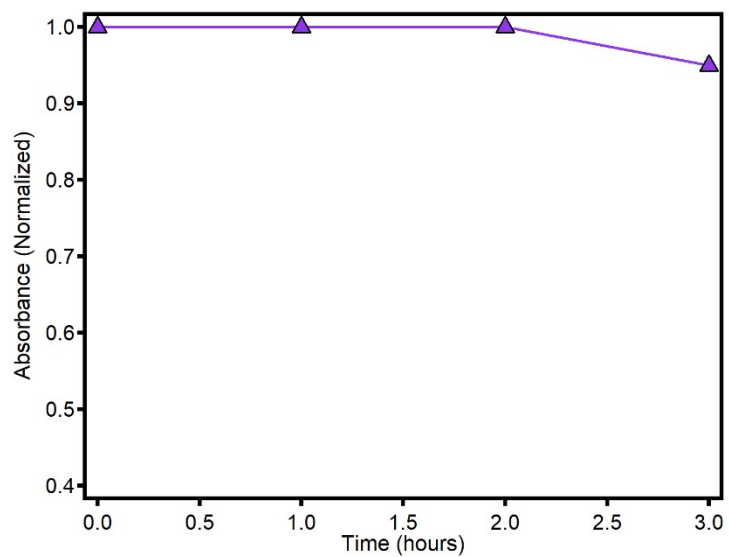
a) GOx



b) GOx & Protease@MIL-101(Al)-NH₂



c) GOx & free protease



S6. References.

- 1 C. Férey, C. Mellot-Draznieks, C. Serre, F. Millange, J. Dutour, S. Surblé and I. Margiolaki, *Science*, 2005, **309**, 2040–2042.
- 2 P. Serra-Crespo, E. V. Ramos-Fernandez, J. Gascon and F. Kapteijn, *Chem. Mater.*, 2011, **23**, 2565–2572.
- 3 T. Roisnel and J. Rodríguez-Carvajal, *Mater. Sci. Forum*, 2001, **378–381**, 118–123.
- 4 V. Agostoni, T. Chalati, P. Horcajada, H. Willaime, R. Anand, N. Semiramoth, T. Baati, S. Hall, G. Maurin, H. Chacun, K. Bouchemal, C. Martineau, F. Taulelle, P. Couvreur, C. Rogez-Kreuz, P. Clayette, S. Monti, C. Serre and R. Gref, *Adv. Healthc. Mater.*, 2013, **2**, 1630–1637.
- 5 R. Anand, F. Borghi, F. Manoli, I. Manet, V. Agostoni, P. Reschiglian, R. Gref and S. Monti, *J. Phys. Chem. B*, 2014, **118**, 8532–8539.
- 6 Sang Woo Cho, N. J. Kim, M. U. Choi and W. Shin, *Acta Crystallogr. D Biol. Crystallogr.*, 2001, **57**, 948–956.
- 7 M. H. M. Olsson, C. R. SØndergaard, M. Rostkowski and J. H. Jensen, *J. Chem. Theory Comput.*, 2011, **7**, 525–537.
- 7 A. W. Götz, M. J. Williamson, D. Xu, D. Poole, S. Le Grand and R. C. Walker, *J. Chem. Theory Comput.*, 2012, **8**, 1542–1555.
- 9 L. Martínez, R. Andrade, E. G. Birgin and J. M. Martínez, *J. Comput. Chem.*, 2009, **30**, 2157–2164.
- 10 W. D. Cornell, P. Cieplak, C. I. Bayly, I. R. Gould, K. M. Merz, D. M. Ferguson, D. C. Spellmeyer, T. Fox, J. W. Caldwell and P. A. Kollman, *J. Am. Chem. Soc.*, 1995, **117**, 5179–5197.
- 11 W. L. Jorgensen, J. Chandrasekhar, J. D. Madura, R. W. Impey and M. L. Klein, *J. Chem. Phys.*, 1983, **79**, 926–935.
- 12 E. Neria, S. Fischer and M. Karplus, *J. Chem. Phys.*, 1996, **105**, 1902–1921.
- 13 V. Kräutler, W. F. Van Gunsteren and P. H. Hünenberger, *J. Comput. Chem.*, 2001, **22**, 501–508.
- 14 X. Wu and B. R. Brooks, *Chem. Phys. Lett.*, 2003, **381**, 512–518.
- 15 D. R. Roe and T. E. Cheatham, *J. Chem. Theory Comput.*, 2013, **9**, 3084–3095.
- 16 W. Kabsch and C. Sander, *Biopolymers*, 1983, **22**, 2577–2637.
- 17 J. Rodríguez-Carvajal, *Phys. B Phys. Condens. Matter*, 1993, **192**, 55–69.
- 18 J. Markwell, *Fundamental laboratory approaches for biochemistry and biotechnology, 2nd edition*, Fitzgerald Science Press, Bethesda Md., 2009, vol. 37.
- 18 A. Cornish-bowden, *Methods Study Mar. Benthos*, 2013, **34**, 1–17.
- 20 S. R. Tello-Solis and A. Hernandez-Arana, *Biochem. J.*, 1995, **311**, 969–974.
- 21 D. Feng, T. F. Liu, J. Su, M. Bosch, Z. Wei, W. Wan, D. Yuan, Y. P. Chen, X. Wang, K. Wang, X. Lian, Z. Y. Gu, J. Park, X. Zou and H. C. Zhou, *Nat. Commun.*, 2015, **6**, 1–8.